Journal of Controlled Release 283 (2018) 269–279

Contents lists available at ScienceDirect

Journal of Controlled Release

journal homepage: www.elsevier.com/locate/jconrel

Predicting drug permeability through skin using molecular dynamics simulation

Magnus Lundborg[a], Christian L. Wennberg[a], Ali Narangifard[a,b], Erik Lindahl[c,d], Lars Norlén[e,f,*]

[a] ERCO Pharma AB, Science for Life Laboratory, Solna, Sweden
[b] Department of Medicine, Solna (MedS), Karolinska Institute, Solna, Sweden
[c] Department of Biochemistry and Biophysics, Science for Life Laboratory, Stockholm University, Stockholm, Sweden
[d] Swedish eScience Research Center, Department of Physics, KTH Royal Institute of Technology, Stockholm, Sweden
[e] Department of Cell and Molecular Biology (CMB), Karolinska Institute, Solna, Sweden
[f] Dermatology Clinic, Karolinska University Hospital, Solna, Sweden

ARTICLE INFO

Keywords:
Skin permeation
Stratum corneum
Drug permeability
Molecular dynamics simulation
Lipids

ABSTRACT

Understanding and predicting permeability of compounds through skin is of interest for transdermal delivery of drugs and for toxicity predictions of chemicals. We show, using a new atomistic molecular dynamics model of the skin's barrier structure, itself validated against near-native cryo-electron microscopy data from human skin, that skin permeability to the reference compounds benzene, DMSO (dimethyl sulfoxide), ethanol, codeine, naproxen, nicotine, testosterone and water can be predicted. The permeability results were validated against skin permeability data in the literature. We have investigated the relation between skin barrier molecular organization and permeability using atomistic molecular dynamics simulation. Furthermore, it is shown that the calculated mechanism of action differs between the five skin penetration enhancers Azone, DMSO, oleic acid, stearic acid and water. The permeability enhancing effect of a given penetration enhancer depends on the permeating compound and on the concentration of penetration enhancer inside the skin's barrier structure. The presented method may open the door for computer based screening of the permeation of drugs and toxic compounds through skin.

1. Introduction

The skin's permeability barrier is essential for preserving body homeostasis and for preventing uptake of harmful substances in the environment. It is located to a ceramide-enriched stacked lamellar lipid structure situated in the intercellular space between the cells of the superficial most part of skin, the stratum corneum. [1] The lamellar lipid structure has a unique molecular organization based on stacked bilayers of fully splayed ceramides with cholesterol primarily located to the ceramide sphingoid side and free fatty acids located to the ceramide fatty acid side [2, 3].

The use of chemicals in society is extensive, leading to human exposure with potentially harmful effects. One route of exposure is through the skin. A better understanding of skin absorption of chemicals may aid the development of a safer chemical environment.

Absorption of chemicals *via* the skin is also of significance for medical drug administration. Transdermal drug administration has a number of advantages compared with conventional per oral administration. By avoiding first passage metabolism in the gastrointestinal tract and liver, and by allowing for a continuous drug administration over days to weeks, medication may be better controlled. This in turn may lead to reduced side effects, more stable dosage levels and increased patient compliance. However, only a handful of drugs can presently be administered through skin, with the limiting factor being the skin's permeability barrier. To create a safe future chemical environment and improve drug administration through skin, there is a need to assess chemicals' skin permeability properties and to predict how these could be altered.

Today, the dominating means of assessing skin permeability to chemicals is by *in vitro/ex vivo* testing. Permeability is commonly assessed using diffusion cells [4], such as Franz cells, consisting of a piece of excised skin (human or animal) separating a donor and a receptor chamber. Diffusion cell experiments are however expensive and time consuming, and the European Union (EU) regulation (76/768/EEC, Feb. 2003) prohibits the use of animal skin for pharmaceutical testing. Furthermore, interpretation of diffusion cell permeability data in terms of *in vivo* skin permeability is not straightforward [5].

During diffusion cell experiments, the skin sample is exposed to the

* Corresponding author at: Department of Cell and Molecular Biology (CMB), Karolinska Institute, Solna, Sweden.
E-mail address: lars.norlen@ki.se (L. Norlén).

https://doi.org/10.1016/j.jconrel.2018.05.026
Received 22 December 2017; Received in revised form 27 April 2018; Accepted 21 May 2018
Available online 01 June 2018

donor and receptor fluids for prolonged time periods (often > 24 h to ensure steady-state conditions during the flux measurements), which might affect the skin sample's molecular structure and permeability. The most commonly used donor and receptor fluid is water, which in itself is a skin penetration enhancer. [6, 7] The effect of hydration on skin permeability is also evident in clinical practice as occlusive dressings that increase the water content of stratum corneum generally dramatically potentiate the effect of drugs locally applied to skin. Furthermore, ethanol, which is a commonly used co-solvent in diffusion cell experiments, also enhances skin permeability. [8] A perturbing effect on the skin sample's permeability barrier structure upon prolonged exposure to water and co-solvents might explain the large variability in skin permeability reported in the literature for individual compounds (e.g., about one order of magnitude for testosterone [9, 10]) as well as the generally higher permeability values reported in *in vitro* (*ex vivo*) diffusion cell experiments compared with *in vivo* measurements [5].

To facilitate drug delivery through skin, penetration-enhancing compounds have been studied extensively. Typical examples are sulfoxides (such as DMSO), Azone (1-dodecylazacycloheptan-2-one or laurocapram), fatty acids (such as oleic acid), alcohols (such as ethanol), or surfactants (such as sodium lauryl sulfate (SLS)). [8] Most penetration enhancers, however, have an unknown mode of action, limiting their use in commercial drug delivery formulations [8].

Various mechanisms of action have been proposed for different chemical penetration enhancers, such as i) altering the solubility of the drug in the donor phase, ii) changing the solubility properties of stratum corneum, iii) modifying the thermodynamic activity of the drug, iv) promoting transport by "dragging" the permeant through the skin, and v) perturbation of the skin barrier's lipid organization (alternative mechanisms summarized in Ref. 8). The last proposal (v) has attracted special attention. Several molecular mechanisms have been proposed, including an increased lipid disorder due to interaction with the skin lipid headgroups or their hydrocarbon tail regions, promotion of lipid phase separation, or removal of barrier lipids by extraction. [8] The complex modes of action of different penetration enhancers are underlined by the fact that an increased stratum corneum lipid disorder does not necessarily correlate with increased flux rates [11], although lipid mobility can at times be linked to skin permeability. [12] For example, using natural abundance ^{13}C polarization transfer solid-state nuclear magnetic resonance (NMR) on porcine stratum corneum, Pham et al. reported that addition of oleic acid ($OA_{C18:1}$) leads to an increased mobility in lipid acyl chain regions and in cholesterol, while it has a negligible effect on the mobility of ceramide headgroups. [12] On the contrary, at high hydration levels, Azone increases the mobility of ceramide headgroups. [12] Drawbacks with skin NMR studies are, however, that the amount of embedded penetration enhancer that actually has been dissolved in the skin sample's lipid structure is difficult to estimate, and that the effect on skin lipid mobility of the added penetration enhancer itself and the effect on skin lipid mobility of a simultaneously altered water activity induced by the added penetration enhancer, cannot be distinguished [12].

One way of investigating the molecular mechanisms behind drug permeation through skin is by *in silico* modeling of skin permeability. A classical approach is by using quantitative structure-activity relationship (QSAR) models, [13] which in this context would be more properly called "quantitative structure-permeability relationship" models, but the term QSAR will still be used herein. A QSAR model mathematically relates a number of physicochemical descriptors to a response. The selection of descriptors usually varies between models, but the partition coefficient (logP) and molecular weight are commonly used, sometimes along with, e.g., the number of hydrogen bond forming groups. The constants, i.e., "weights", in the mathematical formula are trained to achieve a good fit between experimental and predicted data. QSAR models are, however, critically dependent on the quality and applicability domain of the input training set data. [14, 15, 16] QSAR models have proven good at predicting permeability coefficients measured in diffusion cells with reported mean absolute errors as low as 0.09 log units. [17, 18, 19] These data are typically derived from diffusion cell experiments of uncertain relevance for skin permeability *in vivo*. [5, 6] Furthermore, QSAR models cannot be used for predicting drug permeability in a complex context, such as in the presence of penetration enhancers. More complex *in silico* models using a two-dimensional "brick-and-mortar", with parameters for hydration, have performed well in reproducing experimental data with a reported rms error of 0.51 log units [20, 21].

Another approach is investigating the molecular mechanisms behind drug permeation through skin. This can be done by molecular dynamics (MD) simulation by building models and testing their predictive abilities. MD modeling has the advantage over QSAR modeling that information about the molecular mechanisms governing the skin drug permeation process may be obtained. It also allows for broader investigation, and potentially screening, of the transdermal drug delivery process including effects of penetration enhancers, stratum corneum hydration, and partitioning between delivery vehicle and skin. Furthermore, MD simulations do not require any training provided that the biomolecular force fields that govern the atomic interactions are validated. MD simulations make it possible to study a system, and its interactions and properties over time and at a time scale that is not accessible through other means, at an atomic level. One limitation with all-atom MD simulations is, however, that the time scales that can be conveniently simulated are in the range of microseconds. Another challenge is that the output from MD simulations must be validated against reliable experimental data, which are difficult to obtain for biological systems.

Nonequilibrium MD simulations, in which a permeant is pulled in the forward and reverse directions along the reaction coordinate, e.g., across a membrane, using a stiff spring (a strong umbrella potential), is one method for calculating the permeability through a system. [22, 23, 24, 25, 26] This requires extensive sampling, especially through a heterogeneous system with low diffusion, such as the skin barrier lipid model system. The permeant must also be pulled slowly enough to ensure close to equilibrium conditions, and with enough repeats to take into account most important low-energy configurations. If the partitioning between the delivery vehicle and at least one point in the lipid structure is calculated (see Fig. 1) the resulting permeability coefficient will represent the transfer from the delivery vehicle and through the skin, provided that passing the skin lipid model system is the rate limiting step.

Several groups have previously used MD simulations to estimate the skin's permeability using simplified skin barrier models. [27, 28] Interpretation of MD simulation data in terms of relevance for skin permeability may, however, critically depend on the lipid model used. So far, a validated skin barrier lipid MD model has been lacking. Previous simulations for permeation calculations through stratum corneum have used bilayer models with monodispersed (C24:0) ceramides in the hairpin conformation and with excess water on each side of the lipid bilayer structure. [27, 28] Both Das et al. [27] and Gupta et al. [28] used a 1:1:1 system of ceramide NS (C24:0) (for a description of skin ceramide nomenclature see Ref. (29), lignoceric acid (C24:0) and cholesterol. In the study by Das et al. the water $logK_{P_{350K}}$, in cm/h, was ~0.5 (recalculated from reported ΔG and D(z) values) [27], which would correspond to a $logK_{P_{303K}} \sim -1.4$ with temperature corrections according to Eq. 1 (provided there is a linear relationship over the large temperature range) [30]. Gupta et al. report $logK_{P_{310K}}$ (in cm/h) for water of −0.6 [28], which would equate to a $logK_{P_{303K}}$ of −0.9 with the

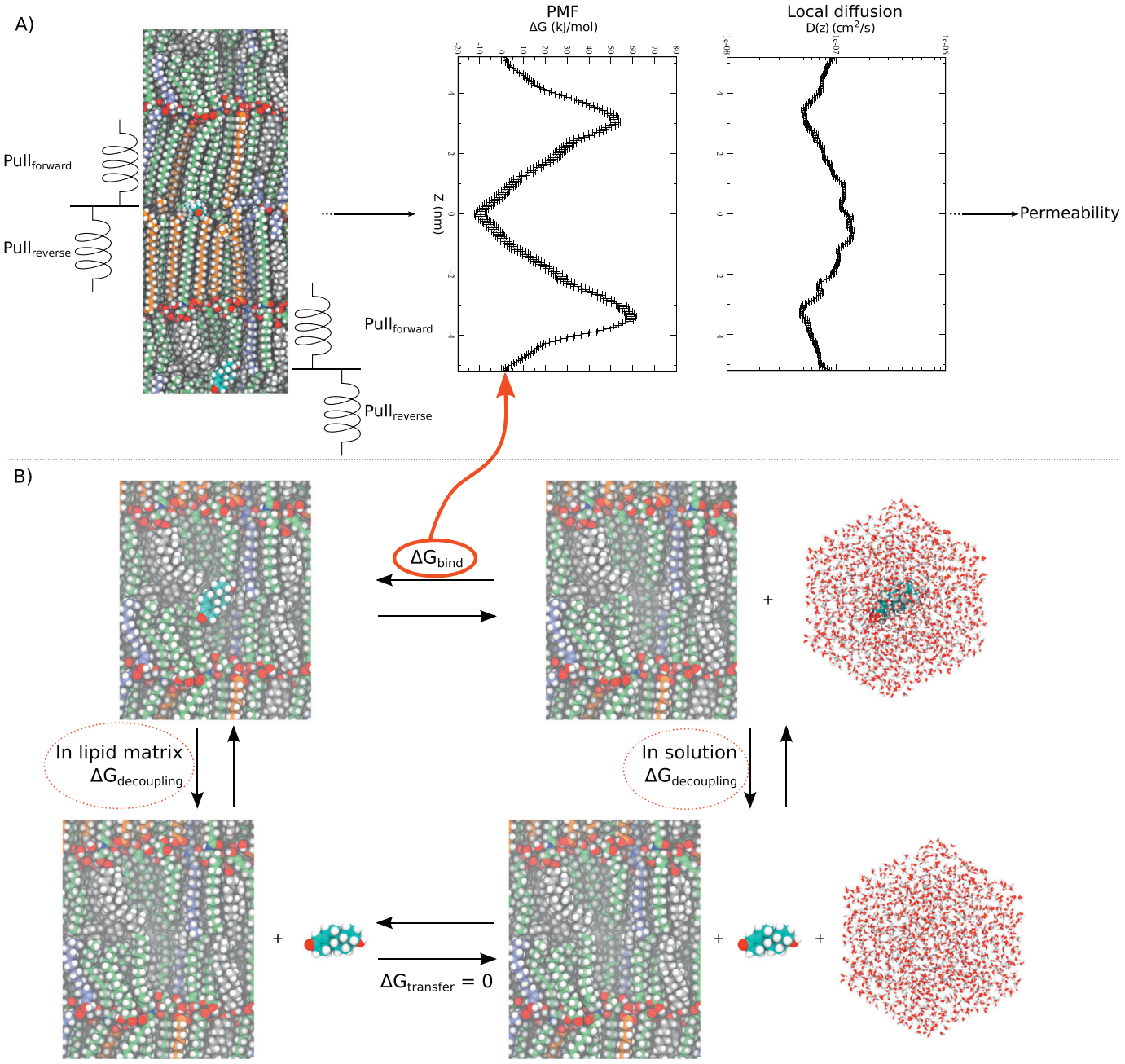

Fig. 1. Outline of the general procedure for calculating the permeability of a ligand through the system. A) Two copies of the ligand (cyan carbon atoms) are grown into the system and its potential of mean force (PMF) and local diffusion coefficient are obtained from forward-reverse nonequilibrium pulling through the system. [22–26, 34] B) The PMF is calibrated by calculating the binding free energy of the ligand, at the position where the PMF starts. The thermodynamic cycle shows that only the hydration free energy, obtained from decoupling the ligand in water, and the interaction free energy of the ligand in the lipid matrix, obtained by decoupling the ligand in the lipid matrix system, are required to calculate the binding free energy of the ligand. (For interpretation of the references to colour in this figure legend, the reader is referred to the web version of this article.)

same correction as above. This is a factor 100 higher than the water permeability of human skin reported from diffusion cell experiments ($logK_{P_{303}}$ − 2.9 cm/h [31, 32]). Besides water, Gupta et al. [28] also reported a higher permeability compared to *in vitro/ex vivo* diffusion cell experiments for most compounds included in their study. Considering the skin membrane is excessively hydrated in diffusion cells, which increases its permeability, [6, 33] and that the skin's lipid structure (modelled in the MD simulations) represents the main permeability barrier, it is anticipated that the real *in vivo* permeability coefficients, and ideally the simulated permeability coefficients, should be lower than those measured in diffusion cells *in vitro*.

Recently, we proposed a new atomistic MD model, validated against near-native high-resolution cryo-EM data from human skin, for the molecular structure and function of the skin's permeability barrier. [3] The new MD model is based on stacked bilayers of fully splayed skin ceramides, cholesterol, free fatty acids, acyl ceramides and water, with 75 mol% of the cholesterol associated with the ceramide sphingoid moiety and 100 mol% of the free fatty acids associated with the ceramide fatty acid moiety, with 5 mol% of acyl ceramides, and with one water molecule per three lipids (ceramide, cholesterol and free fatty

acids), associated with the headgroups. The new model is herein referred to as 33/33/33/75/5/0.3[1].

In this study, we have used the new atomistic MD model for the skin's permeability barrier to calculate the permeability of the stratum corneum's lipid structure to eight reference compounds of differing sizes and physicochemical properties (benzene, codeine, DMSO, ethanol, naproxen, nicotine, testosterone and water). In addition, the effect of five chemical penetration enhancers (Azone, DMSO, oleic acid, stearic acid and water) on the stratum corneum's lipid structure, as well as the effect of four of these permeability increasing compounds (Azone, oleic acid, stearic acid and water) on the permeability of codeine, ethanol, nicotine, testosterone and water, was investigated. The effect of increasing amounts of Azone, as a penetration enhancer, on the permeability of itself was also investigated in order to deduce how easily a penetration enhancer goes through the skin barrier at increasing concentrations.

Moreover, different mechanisms of action are proposed for the five penetration enhancers studied. Water primarily relocates to the lipid headgroup region, but also forms pools at the interfaces between the lipid tails, mainly at the ceramide fatty acid tail interface. The polar groups of Azone, oleic acid and stearic acid are partially associated with the model's lipid headgroups, while the nonpolar groups favor the model's longer ceramide fatty acid chains. However, a significant fraction of the Azone, oleic acid and stearic acid molecules locate to the shorter ceramide sphingoid chains as well as to the interfaces between the lipid chains on both the ceramide fatty acid and ceramide sphingoid sides. This latter phenomenon could be compared to forming a separate phase of the penetration enhancer inside the skin barrier lipid system. The interface between the model's lipid chains is favorable for drug partitioning, and even more so when a penetration enhancer accumulates there. Finally, it is shown that DMSO forms pores through the model system.

2. Results

2.1. Calculated permeability of benzene, codeine, DMSO, ethanol, naproxen, nicotine, testosterone and water through the new MD model of the skin's barrier structure

Physicochemical properties of the tested permeants are shown in the Supplementary Information (Table S1). Experimental permeability coefficients obtained from the literature were acquired at temperatures ranging from 25 to 37 °C. We applied a similar temperature correction of log K_P as Abraham and Martins [30] by adjusting the experimental log K_P values according to:

$$logK_{P_{303K}} = logK_{P_{Texp}} + 0.04 \times (303 - T_{exp}), \quad (1)$$

where $logK_{P_{303K}}$ is the permeability coefficient at 303 K, the temperature at which the MD simulations were run, $logK_{P_{Texp}}$ is the experimental permeability coefficient at the temperature the experiment was performed and T_{exp} is the experimental temperature (in K).

Results from permeability calculations of benzene, codeine, DMSO, ethanol, naproxen, nicotine, testosterone and water using the skin barrier model system (33/33/33/75/5/0.3[2]) are presented in Table 1. Potentials of mean force (PMFs) and diffusion coefficient profiles are shown in Fig. 2. For a comparison between symmetrized and unsymmetrized PMFs see Fig. S1 in the Supplementary Information. In order to evaluate the sensitivity of the permeability coefficient calculations to the skin barrier model system's starting conditions, two additional instances of the skin barrier model system were created. Furthermore, the original instance of the skin barrier model system was equilibrated for 5 μs, instead of ~350 ns. Water permeability coefficients were subsequently calculated for all four instances of the model system. The mean log K_P (in cm/h) for the four instances of the model system was −4.8 and the sample standard deviation was 0.5 (see Table S3).

Table 1
Experimental and calculated permeabilities (log K_P) in cm/h at a pulling speed of 0.2 nm/ns in the 33/33/33/75/5/0.3 [1] model system [3]. Calculated permeabilities after 3, 4 and 5 μs (30–50 pulls in each direction) are presented. The presented uncertainties (indicated by ±) are the standard errors of the calculated log K_P values.

Molecule	log K_{Pexp}	log $K_{P3\mu s}$	log $K_{P4\mu s}$	log $K_{P5\mu s}$
Benzene	−0.8	−1.7 ± 0.2	−1.4 ± 0.2	−1.0 ± 0.2
Codeine	−4.6	−6.4 ± 0.4	−5.9 ± 0.3	−6.4 ± 0.3
DMSO	−3.1	−4.8 ± 0.2	−4.5 ± 0.2	−4.2 ± 0.2
Ethanol	−2.8	−2.7 ± 0.2	−2.9 ± 0.2	−2.7 ± 0.2
Naproxen	−3.0	−3.9 ± 0.2	−4.0 ± 0.2	−4.1 ± 0.2
Nicotine	−1.8	−2.3 ± 0.3	−2.5 ± 0.2	−2.1 ± 0.2
Testosterone	−2.7	−6.2 ± 0.3	−5.8 ± 0.3	−6.1 ± 0.3
Water	−2.9	−4.5 ± 0.2	−4.6 ± 0.2	−4.7 ± 0.1
Mean diff.		−1.34	−1.24	−1.21
Mean abs. diff.		1.39	1.24	1.24
Mean sq. diff.		2.85	2.26	2.60

2.2. Dependence on model structure on the calculated permeability of benzene, codeine, DMSO, ethanol, naproxen, nicotine, testosterone and water

The calculated permeability of the model recently proposed by Lundborg et al. [3] differed significantly from that of an earlier model proposed by Iwai et al. [2]. The Iwai et al. model (Table S2) showed higher permeability coefficients than those reported experimentally in diffusion cell experiments for all studied compounds except for water, while the Lundborg et al. model (Table 1) showed lower permeability values than those reported experimentally for all studied compounds except for ethanol.

2.3. Calculated mechanism of action of the penetration enhancers Azone, DMSO, oleic acid, stearic acid and water on the skin's barrier structure

The five different chemical penetration enhancers Azone, DMSO, oleic acid, stearic acid and water behaved differently in the skin barrier lipid model, as can be seen in Fig. 3 (for lower concentrations see Fig. S2 in the Supplementary Information).

The polar groups of Azone (Fig. 3b), oleic acid (Fig. 3d) and stearic acid (Fig. 3e) were associated with the ceramide headgroup region, as expected, but also with the interfaces between the lipid hydrocarbon chains. At these interfaces, Azone, oleic acid and stearic acid preferably associated with other molecules of their own kind and with the acyl ceramides' linoleic acid chains. The non-polar tails of Azone, oleic acid and stearic acid were generally aligned with the ceramide chains, seemingly favoring the longer fatty acid region, or located in the hydrocarbon interface regions. This agrees with the expected mechanism of a disruption of the skin barrier's lipid packing and with an inhomogeneous distribution of these penetration enhancers in the system, even forming separate phases inside the skin's lipid structure. [8, 35] The MD simulations suggest that Azone, oleic acid and stearic acid are integrated in the lipid barrier in a similar way. The different shapes of the penetration enhancer molecules, and their degree of saturation, determine to what extent they disrupt the skin barrier lipid packing. It has been reported that stearic acid is increasing the skin barrier structure's lipid headgroup mobility slightly, but not the mobility of the lipid chains, whereas oleic acid increases the mobility of the lipid chains and of cholesterol, but not of the lipid headgroups. [12] In the same study it was shown that Azone increases the mobility of lipid chains and cholesterol, and, at higher

[1] Relative composition in molar %: ceramides/cholesterol/free fatty acids/relative amount of cholesterol on ceramide sphingoid side/acyl ceramide EOS (included in rel. Conc. ceramides)/water molecules per lipid.

[2] Relative composition in molar %: ceramides/cholesterol/free fatty acids/relative amount of cholesterol on ceramide sphingoid side/acyl ceramide EOS (included in rel. Conc. ceramides)/water molecules per lipid.

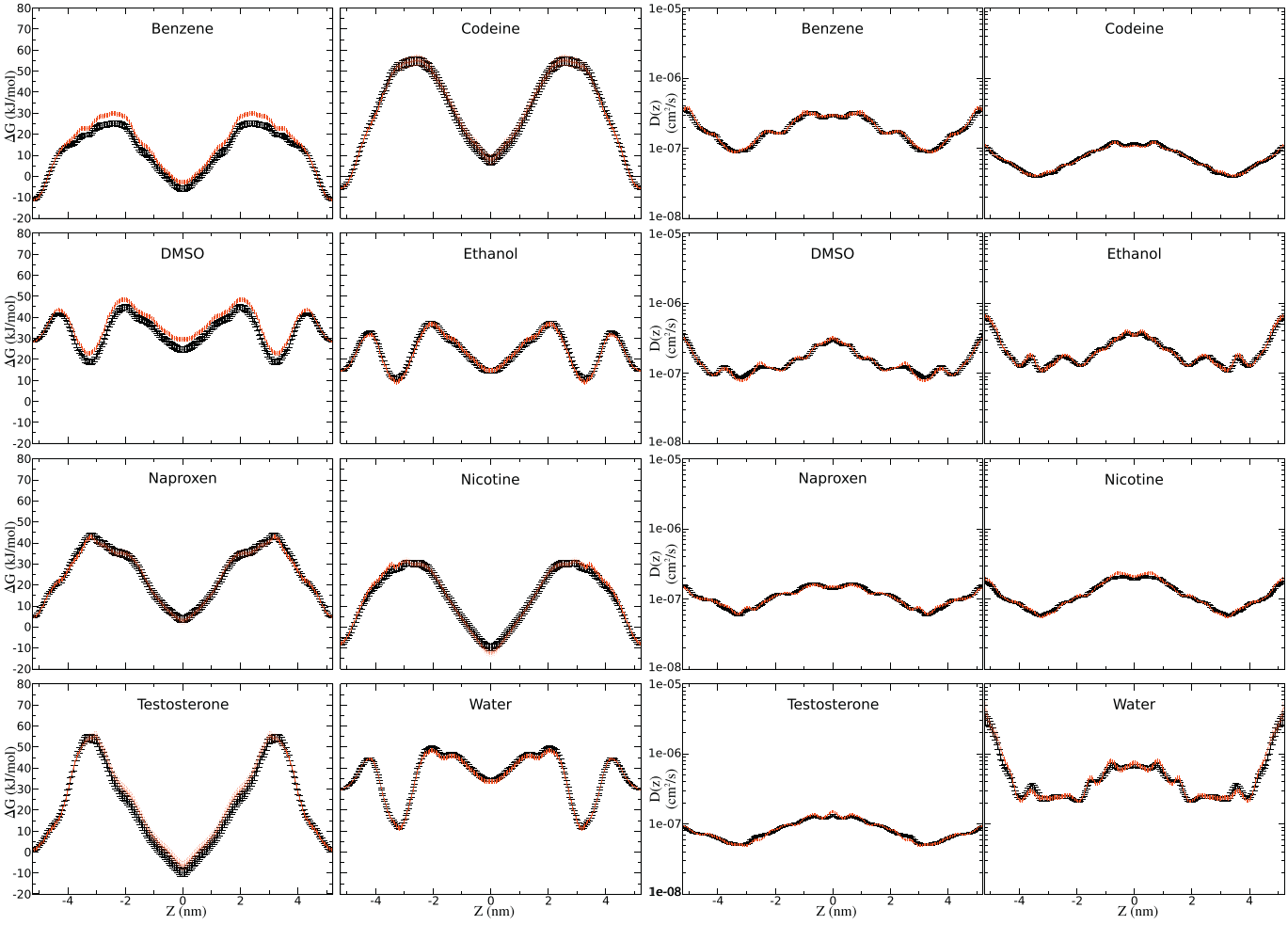

Fig. 2. PMFs (ΔG) and local diffusion coefficients (D(z)) of the studied compounds. The solid black line is the results after totally 5 μs (50 pulls in each direction), whereas the red dashed line shows the results after totally 3 μs. The contributing work is symmetrized to achieve symmetric profiles. The error bars indicate the standard error at each point. The PMFs and local diffusion coefficient profiles are symmetrized. (For interpretation of the references to colour in this figure legend, the reader is referred to the web version of this article.)

hydration levels, also of lipid headgroups. [12] In the simulations performed herein the uncertainty of the headgroup mobility measurements is, however, too large to draw any conclusions (see Table S4).

DMSO initially clustered in the polar lipid headgroup regions and then, over time, spread to the non-polar hydrocarbon chain regions forming pores through the skin barrier lipid system (Fig. 3c). Since DMSO is a good solvent for many different compounds, these pores could explain its penetration enhancing properties. The formation of pores has been the suggested penetration enhancing mechanism for some penetration enhancers [8] including DMSO [36].

In the MD simulations, water molecules were not only associated with the lipid headgroup region, but were also grouped at the interfaces between the non-polar lipid chains. This would improve the general solubility of hydrophilic molecules in the skin's lipid structure and could enhance their permeation. Lipophilic molecules with polar groups, such as most drug molecules, would also have an improved solubility at the interfaces between the lipid chains if there were a separate water partition available to solvate hydrophilic groups. Experimental evidence has shown that water forms microscopic vesicle-like pools without large distortions of the lipid domain [37]. In the MD simulations, small nanoscaled water domains can be observed (Fig. 3f). It has been reported that water can also form pores through the skin's lipid structure, [38] which was not observed in our simulations at concentrations up to 9 wt% of added water. However, at even higher concentrations formation of water pores was seen (Fig. S2g).

2.4. Calculated permeability enhancing effect of the penetration enhancers Azone, oleic acid, stearic acid and water on the permeability of codeine, ethanol, nicotine, testosterone and water

The effect of the penetration enhancers on the permeability coefficient of five compounds is presented in Table 2. It can be observed that excessive hydration has a large impact on the calculated permeability coefficients for all studied compounds. Furthermore, the effect of hydration on permeability is not the same for all five compounds. The effect of hydration is also not linear and peaks at 7 wt% water for all five compounds, although this phenomenon is least pronounced for the permeability of water itself (Table 2). Comparing Azone, oleic acid and stearic acid, stearic acid has a lower effect on the permeability coefficient of the five compounds than does Azone and oleic acid. This may be expected due to stearic acid's saturated aliphatic chain, and has previously been shown experimentally. [39, 40] Furthermore, the permeability-enhancing effect of the different penetration enhancers is compound-dependent and concentration dependent. For example, Azone at higher concentration (9 wt%) is most efficient in increasing the permeability of testosterone, whereas oleic acid raises the pemeability of codeine and nicotine most efficiently, together with 7 wt% water (Tables 2 and S5). However, at lower Azone concentration (5 wt%), oleic acid as well as higher water concentrations (7–9 wt%) are more efficient than Azone also in increasing the permeability of testosterone.

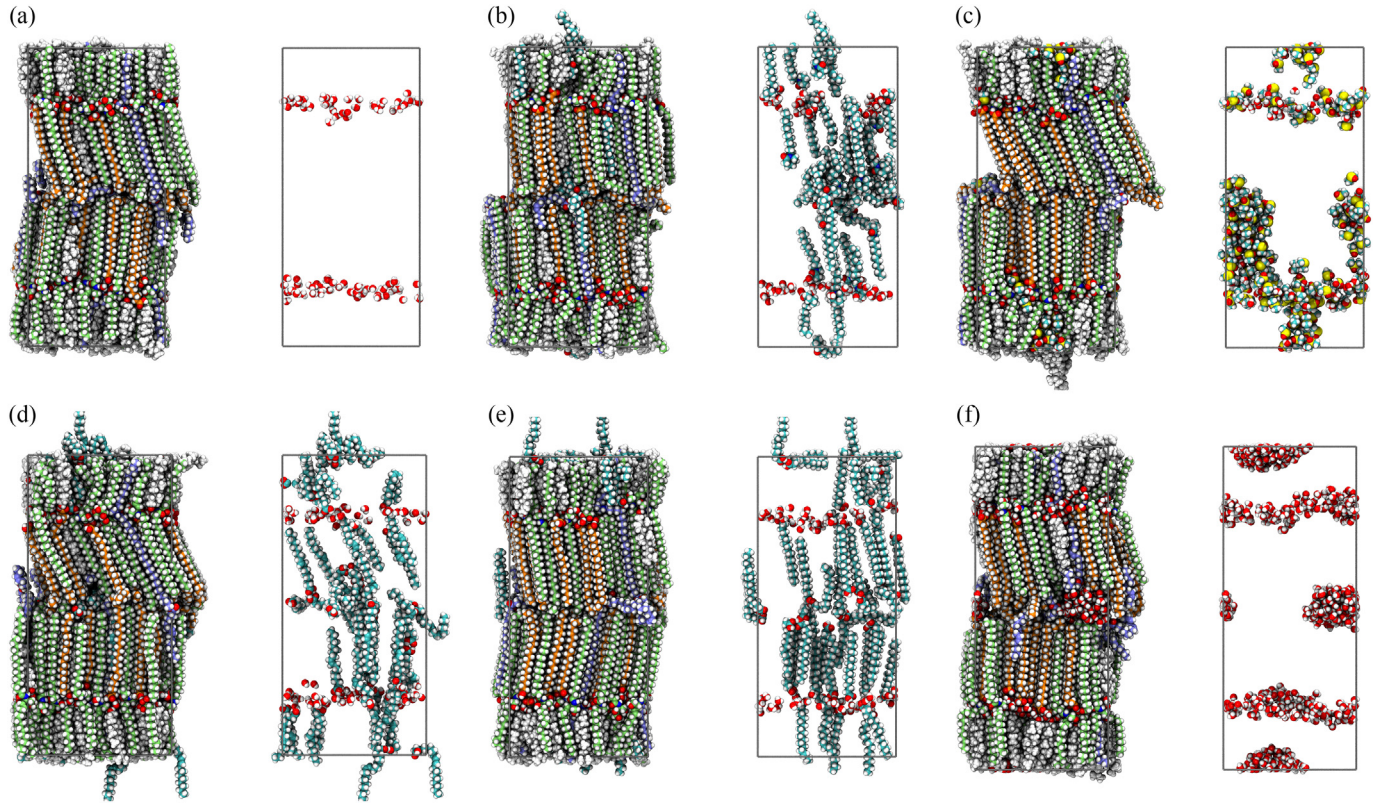

Fig. 3. Effect of penetration enhancers on the structure of the skin barrier lipid model system. The concentration of the penetration enhancers is approximately 9 wt %. (a) shows the system without penetration enhancers. The molar ratios in (b)-(f) are: (b) Azone 0.5/CER, (c) DMSO 2/CER, (d) oleic acid 0.5/CER, (e) stearic acid 0.5/CER and (f) water 8/CER. In each subfigure (a–f) the first figure shows the whole system, while the second figure shows the permeability enhancing molecules and the water in the system. All carbon atoms in non-acyl ceramides are green, in acyl ceramide EOS light blue, in free fatty acids orange and in cholesterol grey. The rest of the atoms are colored according to atom types (oxygen: red, nitrogen: blue, sulfur: yellow, hydrogen: white). For "Water 8/CER" the total amount of water present in the system is the added amount of added water in addition to the 1 water/ceramide that was already present in the reference system [3]. (For interpretation of the references to colour in this figure legend, the reader is referred to the web version of this article.)

2.5. Permeability of Azone, in the presence of itself as a penetration enhancer

The calculated permeability of Azone in a skin lipid model system with increasing amounts of Azone preexisting in the model system is presented in Table 3. Counting the pulled Azone molecules as one molecule (since they cannot interact with each other) and counting the Azone molecules inserted as penetration enhancers individually, the corresponding Azone concentration of a topical formulation can be estimated based on the partition coefficient of Azone throughout the Azone enriched skin barrier lipid model system. The amount of Azone partitioned into the skin lipid model system was calculated from its PMF (that corresponds inversely to the partition function).

As can be seen in Table 3, 9 wt% Azone in the skin lipid model system (corresponding to approximately 12 wt% in the topical formulation) has the highest permeability, followed by 2 wt% Azone in the system (corresponding to ~3 wt% in the topical formulation). At 5 wt% in the system (corresponding to ~8 wt% in the topical formulation) the permeability is lower, but still higher than in the skin lipid model without any added Azone as penetration enhancer.

Table 2
Calculated permeability coefficients (in cm/h), of five compounds, with penetration enhancer in the main model system [3]. The total simulation time for each experiment was 3 μs (30 pulls in each direction). The presented uncertainties (indicated by ±) are the standard errors of the calculated log K_P values. The Azone concentrations equate to 1/2 and 1/4 Azone molecules per ceramide or 1/6 and 1/12 Azone molecules per lipid. The oleic acid and stearic acid concentrations equate to 1/2 molecules per ceramide or 1/6 molecules per lipid. The water concentrations equate to 8, 6, 5 and 4 extra water molecules per ceramide or 8/3, 2, 5/3 and 4/3 extra water molecule per lipid.

Perm.	Codeine	Ethanol	Nicotine	Testosterone	Water
Enhancer	log K_P	log K_P	log K_P	log K_P	log K_P
Azone 9 wt%	−2.8 ± 0.4	−0.6 ± 0.2	−1.2 ± 0.3	0.2 ± 0.3	−2.4 ± 0.2
Azone 5 wt%	−4.8 ± 0.3	−1.3 ± 0.2	−1.8 ± 0.2	−3.5 ± 0.4	−3.9 ± 0.2
Oleic acid 9 wt%	−1.4 ± 0.4	−0.7 ± 0.3	−0.2 ± 0.3	−1.1 ± 0.3	−2.9 ± 0.2
Stearic acid 9 wt%	−5.1 ± 0.3	−1.5 ± 0.3	−1.1 ± 0.3	−4.0 ± 0.4	−3.7 ± 0.2
Water 9 wt%	−2.7 ± 0.3	−0.3 ± 0.2	−0.2 ± 0.2	−1.5 ± 0.3	−2.2 ± 0.1
Water 7 wt%	−0.4 ± 0.2	0.2 ± 0.1	−0.0 ± 0.1	−0.2 ± 0.2	−2.0 ± 0.1
Water 6 wt%	−3.0 ± 0.3	−2.2 ± 0.1	−1.6 ± 0.2	−3.1 ± 0.3	−3.8 ± 0.1
Water 5 wt%	−3.7 ± 0.2	−1.9 ± 0.1	−0.6 ± 0.1	−4.5 ± 0.2	−3.8 ± 0.1
None	−6.4 ± 0.4	−2.7 ± 0.2	−2.3 ± 0.3	−6.2 ± 0.3	−4.5 ± 0.2
Experimental	−4.6	−2.8	−1.8	−2.7	−2.9

Table 3
Calculated permeability coefficients (in cm/h) of Azone through the main model system [3], with increasing amounts of Azone. The approximate concentration of Azone in the formulation is based on the partition coefficient (from the PMF) and the concentration of Azone in the lipid system. The total simulation time for each experiment was 3 μs (30 pulls in each direction). The presented uncertainties (indicated by ±) are the standard errors of the calculated log K_P values. The Azone concentrations in the lipid system correspond to 1/20, 1/10, 1/4 and 1/2 Azone molecules per ceramide molecule or 1/60, 1/30, 1/12 and 1/6 Azone molecules per lipid.

Azone concentration	Corresponding Azone concentration	
in MD model system	in a hypothetical topical formulation	log K_P
0 wt%	0.4%	−4.0 ± 0.3
1 wt%	2.2%	−2.2 ± 0.3
2 wt%	3.1%	−0.8 ± 0.3
5 wt%	8.1%	−2.6 ± 0.4
9 wt%	11.8%	2.1 ± 0.2

3. Discussion

The stratum corneum constitutes a barrier towards penetration of chemicals from the environment into the body. In general, small (molecular weight below 500 Da) and relatively lipophilic (log $P_{octanol–water}$ 1–3) compounds with a low melting point have properties optimal for skin permeation. [41] However, most drugs have low skin permeability and can therefore not be administered topically. To facilitate administration of drugs through skin, penetration enhancers are routinely employed. Their mechanisms of action are, however, not well understood, [8] and delivery of larger and more hydrophilic drugs remains a challenge.

Drug permeability through skin is currently routinely approximated using mathematical models such as QSAR (or QSPR) models. [42] However, the effects on drug permeability of penetration enhancers, or of modified skin hydration, are difficult to account for in these models. [42] Molecular dynamics (MD) simulation has previously been used to calculate permeability coefficients through simplified skin lipid model systems emulating the skin's barrier. However, the calculated permeability coefficients have been overestimated several orders of magnitude compared to skin permeability coefficients measured *in vitro/ex vivo* in diffusion cells, [27, 28] that in turn are expected to overestimate the real *in vivo* skin permeability coefficients by an order of magnitude [6, 33].

Using a recently proposed skin barrier MD model [3], validated by cryo-EM, the relative values of the calculated drug permeability coefficients largely reflect those obtained from diffusion cell experiments *in vitro*. The absolute values of the calculated permeability coefficients are in general lower than those obtained from corresponding diffusion cell experiments (more negative log K_P values) (Table 1). This could be explained by the excessive hydration of the skin membrane in the diffusion cell. A tenfold increase in skin permeability induced by water exposure has been reported, suggesting that results from diffusion cells cannot be interpreted blindly with respect to skin permeability *in vivo*. [6, 33] Since the permeability calculations are based only on the main barrier in skin the resulting permeability coefficients are anticipated to be lower than measurements from diffusion cells. The calculated permeability coefficient of ethanol was slightly higher or equal to diffusion cell measurements. One possible explanation for this could be that the nonpolarizable CGenFF/MATCH forcefield [43, 44] has difficulties reproducing ethanol (a small amphiphilic molecule) properties. A higher concentration of the permeant in the simulated delivery vehicle (pure water in this study) would also lower the permeability coefficient since that would increase the free energy of transfer from the delivery vehicle into the skin barrier model system. It is also possible that longer permeability calculations (more pulls through the system) would further improve the results.

The simulated behaviors of different penetration enhancers in the new skin barrier lipid model system agree with published observations from skin. However, the lack of quantitative reference data defining the distribution of the penetration enhancers *in vivo*, or *in vitro/ex vivo*, inside the skin's lipid structure, makes it difficult to draw any definite conclusions from the simulation experiments. For example, it is possible that, for some penetration enhancers, more enhancer molecules would become incorporated in the lipid chains of the model system with longer equilibration times. Therefore, it cannot be stated that the snapshots in Fig. 3 necessarily reflect the situation *in vivo*, but they may indicate how penetration enhancers work and organize themselves in different ways in the skin's barrier structure.

That Azone and oleic acid disrupt skin lipid packing, as well as form a separate phase within the stratum corneum, has been reported before. [8, 35, 45] Likewise that DMSO forms pores within the stratum corneum [36] and extracts lipids from it [46, 47]. Pore formation by DMSO has also been shown in MD simulations of ceramide bilayers in water. [48] In an MD simulation, forming pores can be considered equivalent to extracting lipids from the system, considering that MD simulations do not allow removing molecules.

When adding water as a penetration enhancer to the model system, the calculated drug permeability values approach the measured permeability values obtained from diffusion cell experiments (in which the skin membrane is exposed to water for days). The amounts of water that become incorporated in the skin membranes during diffusion cell experiments have so far not been determined experimentally. According to our calculations, it may be in the range of 5–6 wt% extra water (in addition to the small amounts of water that is an integrated part of the skin's lipid structure [3]) (Table 2).

The effect of water on the model system's permeability is large and complex, and depends on the permeant (Table 2). Multiple local permeability maxima for water as a function of model system water content has been observed previously. [3] In this previous study [3], all water molecules were inserted by the lipid headgroups, whereas in the present study the added water was inserted throughout the model system, followed by MD equilibration to let the water molecules redistribute (e.g., to the model systems's lipid headgroup regions). The previous study [3] showed that 1–3 wt% water (0.3–0.7 water molecules per lipid) associated with the lipid headgroups gave a *lower* water permeability than did 0 wt% water and 4 wt% water (1.0 water molecules per lipid), respectively [3]. Furthermore, 5 wt% water (1.3 water molecules per lipid) resulted in a *higher* permeability than did 6 and 7 wt% water (1.7 and 2.0 water molecules per lipid), and that 10 wt% water gave the highest permeability. Analogously, in this study, a local maximum in water permeability was observed at 7 wt% water *added* to the model system (Table 2), i.e. at 8 wt% water in total. After MD equilibration, the amount of water associated with the lipid headgroups was a little more than 5 wt%. Thus, the, in the present study, observed local maximum in water permeability at 7 wt% water added to the system (i.e., with 5 wt% water associated with the model system's lipid headgroups) is in agreement with what was reported in the previous study. [3] In addition, the present study shows that the same, or an even more pronounced, local maximum in permeability is also observed for all the other tested compounds (codeine, ethanol, nicotine, testosterone) at 7 wt% water added to the model system, although the effect is least pronounced for nicotine (Table 2).

There is not much published reference drug permeability data obtained from skin in the presence of chemical penetration enhancers. Qualitative comparisons can still be made to diffusion cell data, keeping in mind that *in vivo* permeabilities are expected to be lower. This can be combined with observations regarding the relative effects of penetration enhancers in experimental studies and using *in silico* simulations. It is noted that the calculated permeabilities increase significantly when adding Azone, oleic acid or water, and to a lesser extent when adding stearic acid, to the model system. Stearic acid is not as strong a penetration enhancer as oleic acid, but has been shown to increase the

permeability of some permeants. [39, 40] Due to its high melting point it is practically difficult to incorporate high concentrations of stearic acid in skin. The experimental observation that stearic acid is not as potent in enhancing drug permeability as the other penetration enhancers is thus confirmed *in silico*. An exception is for nicotine permeability, in which case the pearmeability enhancing effect of stearic acid is comparable with that of Azone (Table 2).

A complication for *in silico* screening of the skin permeability enhancing effects of penetration enhancers is that the apparent concentration of penetration enhancers present in the skin's permeability barrier is difficult to determine experimentally *in vivo* and *in vitro*. *In vivo* there will likely be a penetration enhancer concentration gradient present over the skin's lipid structure, and the skin's permeability coefficient will in that case be mainly determined by the regions with low penetration enhancer concentration. In this study the model systems were run in a periodic simulation box, and, presumably, with higher penetration enhancer concentrations compared to the *in vivo* situation, especially for stearic acid with its high melting point. This means that the effect on drug permeability of penetration enhancers may likely be more pronounced in this study compared with in the *in vivo* situation.

Speculatively, by estimating the penetration enhancer concentration present in the skin's lipid structure *in vivo* after topical application, based on the topical formulation's penetration enhancer concentration and the penetration enhancer's partition coefficient between the formulation and the skin's lipid structure, and using that estimated penetration enhancer concentration as input for the MD simulations of drug permeability, the correspondence between *in silico* and *in vivo* data may be further improved.

The approximate penetration enhancer concentration in a hypothetical topical formulation may be estimated based on the simulated model system's penetration enhancer concentration and the amount of penetration enhancer molecules partitioned into the model system calculated from the model system's PMF (that corresponds inversely to the partitioning function).

Such estimations of Azone concentration in hypothetical topical formulations are presented in Table 3. The Azone permeability increase recorded upon adding Azone as a penetration enhancer was largest at a concentration roughly corresponding to 12 wt% in the corresponding hypothetical topical formulation (based only on the partitioning profile, from the PMF, between a water vehicle and the lipid model system). However, a hypothetical topical formulation Azone concentration of 3% was more efficient in increasing Azone permeability than a concentration of 8%. This may be compared to real topical formulations where Azone is typically used in concentrations ranging from 0.1 to 5% (Table 3), where Azone has been found to be most effective. [8] At concentrations of 12% Azone in the formulation, the calculated permeability coefficient was drastically increased. However, *in vivo*, this could, at least partly, be countered by an increased Azone solubility in the topical formulation.

In conclusion, simulated changes in the PMF and the local diffusion coefficient of a drug upon addition of a penetration enhancer may give detailed information about how skin permeability could be modified by penetration enhancers. MD simulation may thus be used to screen how different penetration enhancers may be combined to optimize the skin's permeability for a specific drug. Accounting both for i) a drug's free energy of transfer (the partitioning) from a topical formulation to the skin's lipid structure, and for ii) the combined penetration enhancing effects of multiple formulation ingredients, may make it possible to screen *in silico* how compositional changes made to a topical formulation could affect the delivery of a drug through skin. Furthermore, a modified solubility in the pharmaceutical formulation could possibly explain why some penetration enhancers, e.g. Azone and oleic acid, are reported to be more effective at low concentrations than at high concentrations. Such solubility calculations may be called for in future studies.

4. Methods

4.1. Molecular dynamics simulations

All simulations were performed using GROMACS 5.0 [49, 50] using the Verlet cutoff scheme, updating the pair list every 20 steps (automatically changed to every 40 steps). Van der Waals interactions had a cutoff of 1.2 nm with a smooth force-switch from 1.0 nm to 1.2 nm. The simulations were run without a dispersion correction for energy and pressure to compensate for interactions outside the cutoff. Coulomb interactions were calculated using PME [51] with a radius of 1.2 nm. Hydrogen bonds were constrained using the P-LINCS algorithm [52, 53]. TIP3P [54] parameters were used for water molecules. For the lipid molecules the CHARMM36 lipid force field [55, 56] was used. Ceramide parameters were modified to more accurately reproduce the ceramide NP crystal structure, [57] as described in Ref. 3.

The 33/33/33/75/5/0.3 model system, as well as the Iwai model system, were the same systems as presented previously. [3] Two additional instances of the 33/33/33/75/5/0.3 model system were built, in the same way as presented before, [3] in order to evaluate how sensitive the permeability calculations were to the 33/33/33/75/5/0.3 model system's starting conditions. The original instance of the 33/33/33/75/5/0.3 model system was further equilibrated for a total of 5 μs (instead of ~350 ns). Water permeability coefficients were subsequently calculated for all four instances of the 33/33/33/75/5/0.3 model system (Table S3). The mean and the standard deviation of the water permeabilities were calculated from the log K_P values rather than the K_P values since the permeability depends expontially on ΔG (Eq. 7).

All images representing molecules were prepared using Tachyon [58] in VMD [59].

4.1.1. Permeability MD simulations

Permeabilities of benzene, codeine, DMSO (dimethyl sulfoxide), ethanol, naproxen, nicotine, testosterone and water were calculated using the forward-reverse (FR) method proposed by Kosztin et al. [25] (see 4.1.2 below).

Except for water, for which TIP3P parameters were used, CGenFF [43] parameters were generated using STaGE [60], which in turn uses Open Babel [61] and MATCH [44] to generate GROMACS topologies.

The simulations were run using Copernicus [62, 63] to setup the systems and distribute the simulations to multiple workers running GROMACS 5.0 [49, 50]. For each pulling simulation, in the forward and reverse direction, two molecules were inserted in the lipid matrix model (output from production MD simulation of the 33/33/33/75/5/0.3 system [3]) at random lateral positions, one at the interface between the ceramide sphingoid chain moieties and the other at the interface between the ceramide fatty acid chain moieties. The molecules were inserted using the *gmx insert-molecules* command with *scale* = 0.275 and trying to insert it within a distance of 2.0 nm from the randomly selected position in the *x* and *y* dimensions and 0.1 nm in the *z* dimension. If it was not possible to fit the molecule in 30,000 attempts a new random position was chosen. Thereafter the inserted molecules were grown into the system by slowly turning on the interactions with their surroundings using the decoupling options in GROMACS, starting at *lambda* = 0.75 and linearly going to *lambda* = 0, where *lambda* = 1 means no van der Waals or Coulomb interactions with the rest of the system, over 50 ps.

After additional equilibration (1 ns) the molecules were pulled in the forward and reverse directions (increasing and decreasing *z* coordinates) from the same starting position in 50 ns, giving speeds of approximately 0.2 nm/ns, and a spring force constant of 15,000 kJ mol^{-1} nm^{-2} for benzene, DMSO, ethanol and water and a spring constant of 40,000 kJ mol^{-1} nm^{-2} for codeine, naproxen, nicotine and testosterone. In general the higher spring force constant the better, but a too high spring constant risks crashing the simulations.

The simulations were performed using a leap-frog stochastic

dynamics integrator at a temperature of 303.15 K. The pressure was kept using a semiisotropic Parrinello-Rahman barostat [64], with 0 compressibility in the z direction.

The simulations were repeated, at random starting positions, to give a total simulation time of 3–5 μs (30–50 pulls in each direction), i.e., the pulled molecules starting from 30 to 50 different positions in the system.

4.1.2. Calculating the permeability coefficient

Based on the Crooks fluctuation theorem [22, 23] Kosztin et al. proposed the forward-reverse (FR) method [25] where $\Delta G(z)$ is the difference in free energy – forming the PMF (potential of mean force) along the *reaction coordinate* z, and W_d is the dissipative work:

$$\Delta G(z) = \frac{\langle W_F \rangle - \langle W_R \rangle}{2} \tag{2}$$

and

$$\langle W_d \rangle = \frac{\langle W_F \rangle + \langle W_R \rangle}{2}. \tag{3}$$

W_F and W_R are the work done in the forward and reverse directions, respectively. In this work the permeability coefficient was calculated using nonequilibrium forward-reverse simulations [34] and results weighted using the *Brownian Dynamics Fluctuation Dissipation Theorem* (BD-FDT) [26]:

$$e^{-\beta \Delta G(z)} = \frac{\langle e^{-\beta W_F/2} \rangle}{\langle e^{-\beta W_R/2} \rangle}, \tag{4}$$

and applying the same weighting method to the dissipative work gives:

$$e^{-\beta \langle W_d \rangle} = \langle e^{-\beta W_F/2} \rangle \times \langle e^{-\beta W_R/2} \rangle, \tag{5}$$

where $\beta = (k_B T)^{-1}$, k_B is Boltzmann's constant, $\langle \ldots \rangle$ is an average over the ensemble of nonequilibrium trajectories. The position-dependent diffusion coefficient along the reaction coordinate, $D(z)$, is

$$D(z) = \frac{k_B T v}{dW_d/dz}, \tag{6}$$

where v is the pulling speed. The permeability, P, and the resistivity, R, are calculated as follows [65]:

$$\frac{1}{P} = R = \int_{z_1}^{z_2} \frac{e^{\beta \Delta G(z)}}{D(z)} dz. \tag{7}$$

This method requires that the molecules are pulled through the system with a high spring force constant, k, to satisfy the *stiff-spring approximation* [24, 66]. The force constant is thus dependent on the resolution of the PMF, the size of the pulled molecule and the viscosity of its surroundings. [25] The results in this study are obtained using an umbrella pulling force constant of 15,000 kJ mol^{-1} nm^{-2} for benzene, DMSO, ethanol and water and 40,000 kJ mol^{-1} nm^{-2} for the larger compounds. We found that a force constant of 15,000 kJ mol^{-1} nm^{-2} could be used with molecules with a mass $\lesssim$ 100 g/mol. For larger molecules the higher k was used. We have not thoroughly studied the effect of the force constant. It is possible that a force constant of 15,000 kJ mol^{-1} would be sufficient also for the larger molecules. A higher spring constant ensures that the pulled molecule is close to the spring position, but small molecules in regions with low resistivity, e.g. in water, risk exceeding the overdamped limit of the pull force, [66] which can cause instabilities in the simulations. A constraint could also be used for pulling to avoid having to determine what k to use, but that has not been extensively tested yet.

In this paper, the work was calculated based on the distance traveled by the spring, rather than the position of the pulled particle, as done by e.g. Kosztin et al. [25], and the average force exerted by the spring over 100 MD steps (200 fs). The coordinates of the pulled molecules and the applied forces were written every MD step, but afterwards the coordinates every 10,000 steps and the average force over 100 steps were retained for the analyses. The coordinates of the pulled molecules were not used during analysis, since the position of the umbrellas can be calculated based on their starting position and the pull velocity.

The reaction coordinate was divided into 200 segments to group the performed work throughout the system. The work required to pull the spring through each segment was stored. The values were stored separately depending on if the molecule was pulled in the forward or reverse direction. For every separate pulling MD simulation one work value was stored per segment.

The zero point of the PMF (potential of mean force), for transport through the membrane, was set by calculating the free energy difference between the permeant being solvated in water and being embedded in the membrane at the interface between the sphingoid side chains, i.e. the transfer free energy from the vehicle into the membrane. For the hydration free energy calculations the water around the solute filled a dodecahedron shaped periodic box with at least 1.4 nm from the box edges to the solute. The solvation free energy calculations were performed using the free energy module of Copernicus, which runs GROMACS MD simulations, in which interactions between a molecule and its surroundings are decoupled and the free energy of decoupling is calculated using the Bennett Acceptance Ratio (BAR) method. [67] Copernicus automatically optimizes the lambda point distributions for the decoupling of the molecule, starting from 11 lambda points each for decoupling Lennard-Jones and Coulomb interactions. [60, 62] The free energy module runs the calculations in iterations, herein 3 ns per iteration, and after each iteration calculates the free energy and its estimated statistical error. If more iterations are required to reach the requested statistical error the lambda points can also be redistributed. In the bound state (when the ligand was inside the membrane) an umbrella potential, with a force constant of 50 kJ mol^{-1} nm^{-2}, was applied in the Z directions to keep the ligand from drifting through the system when it was decoupled. However, since the permeability of the lipid system is so low the actual force required to keep the ligand in place was low and was not compensated for afterwards. In the future this could be done to possibly improve the zero point of the PMF.

Three calculations were run to calculate the free energy of the hydrated state (in a water box with at least 1.4 nm between the ligand and the box edge), running until the estimated statistical error was not more than 0.25 kJ mol^{-1}. For the bound state six simulations were run to calculate the free energy of the bound state without penetration enhancers and four simulations in the systems with incorporated penetration enhancers, in order to reduce computation times. In both cases requiring a statistical error of no more than 0.50 kJ mol^{-1} in each run. The hydration free energy and bound free energies were set to the Boltzmann weighted average of the three and six (four if running with penetration enhancers) simulations, respectively, and the standard error of the weighted mean. The zero point of the PMF, or the free energy of transfer from the water vehicle into the interface between the ceramide sphingoid chains of the system, was calculated as:

$$\Delta G_{transfer} = \Delta G_{bound} - \Delta G_{hydration} \tag{8}$$

The standard error of the PMF and the local diffusion constant was approximated by bootstrapping the work in each bin, at $p = 0.32$ (68% confidence) and also including the standard error of the binding free energy, by error propagation (using the Uncertainties package in Python).

The resistivity profiles were symmetrized around (approximately) $z = 0$ (center of the membrane) to enhance the sampling. When symmetrizing the data, the PMF was allowed to roll up to 1/8 of the system size to find the minimum difference between the two halves, in order to avoid large difference in case the PMF was not perfectly centered. The work segments were then rolled accordingly and then symmetrization was performed by combining the forward work in each segment with the reverse work of its mirrored segment and *vice versa* for the reverse work. Then the PMF and dissipative work were calculated using these

symmetrized forward and reverse work segments and the error calculated using bootstrapping as above. The uncertainties, i.e., the standard errors, of the calculations only take the statistical error into account. Thus, it cannot account for insufficient sampling. It is therefore expected that the true standard errors are slightly higher.

4.1.3. Permeability in the presence of penetration enhancers

Azone, DMSO, oleic acid, stearic acid and water were used to to study the effect of penetration enhancing compounds on the skin's lipid structure. Stearic acid was used as a control as it is not expected to affect the permeability of the system as much as the other penetration enhancers. [12, 39, 40] The penetration enhancer molecules were inserted into the system (output from production MD simulation of the 33/33/33/75/5/0.3 system [3]) at different concentrations using the *gmx insert-molecules* command with 10,000 tries before giving up. The molecules were inserted at random coordinates. The van der Waals radii of the molecules were scaled by 0.375 from the start. If the requested number of molecules could not be inserted the scaling factor was reduced in steps of 0.05 until the requested number of molecules could be inserted, but no lower than 0.275, at which point 50,000 tries were attempted. The *-allpair* option was also used to avoid memory leaks.

Subsequently, energy minimization, equilibration and production stages were performed. They were the same as described in 4.1.1, but with the exception that the last equilibration stage, without restraints, was divided into three parts: 50 ns at 303.15 K, 150 ns at 318.15 K and 50 ns at 303.15 K. The reason for this temperature increase was to speed up the equilibration of the system.

The resulting output systems of those simulations were used as input systems for new permeability calculations of codeine, ethanol, nicotine, testosterone and water, selected both to represent a large range of log $P_{octanol-water}$ and to represent compounds relevant for transdermal drug administration.

The simulations were run for a total of 3 μs (30 pulls in each direction). The free energy of the "bound" state in the skin barrier lipid models between the ceramide sphingoid chains was based on four free energy calculations. The Boltzmann weighted average of the four simulations was used to calculate the zero point of the PMF, or the transfer free energy from water into the lipid models, as described in 4.1.2 above.

4.1.4. Permeability of Azone, in the presence of itself as a penetration enhancer

Skin barrier lipid model systems with Azone inserted as a penetration enhancer, at concentrations 1, 2, 5 and 9 wt% (0.05, 0.1, 0.25 and 0.5 Azone molecules per ceramide molecule) were prepared as described in 4.1.3 above. The permeability coefficients of Azone through the systems with four different concentrations of Azone already inserted, as well as through the reference system without any pre-inserted Azone, were calculated. The corresponding amount of Azone in a formulation was approximated from on the concentration of Azone in the lipid matrix and the partition coefficient between water and the lipid system, based on the PMF profile through the system according to:

$$logP = \frac{-\Delta G_{transfer}}{RTln10} \quad (9)$$

Author contributions

The molecular systems were generated by M.L. and A.N. The MD simulations were run by M.L. and C.W. Permeability calculations, and related method development, were done by M.L. and C.W. The project and experiments were planned by L.N., M.L., C.W., A.N. and E.L. The article was written by M.L., L.N., C.W., E.L. and A.N.

Acknowledgements

The MD simulations were performed on resources provided by the Swedish National Infrastructure for Computing (SNIC) at PDC Centre for High Performance Computing and by ERCO Pharma AB. ERCO Pharma AB, the Welander foundation, Svenska läkaresällskapet, Oriflame, Shiseido Japan, LEO Pharma, the Wenner-Gren foundation and Vetenskapsrådet are acknowledged for generous financial support. We want to thank Berk Hess for valuable suggestions and ideas.

Declaration of conflicts of interest

This work is presented, in parts, in an application for a European patent with application number PCT/EP2017/076237 and title "SKIN PERMEABILITY PREDICTION".

The work presented herein was essentially funded by ERCO Pharma AB. L.N., M.L., A.N. and C.W. have stock options in ERCO Pharma AB. M.L., A.N. and C.W. are employed by ERCO Pharma AB.

Appendix A. Supplementary data

Supplementary data to this article can be found online at https://doi.org/10.1016/j.jconrel.2018.05.026.

References

[1] P. Elias, K. Feingold, J. Fluhr, Skin as an organ of protection, in: I.M. Freedberg, A.Z. Eisen, K. Wolff, K.F. Austen, L.A. Goldsmith, S.I. Katz (Eds.), Fitzpatrick's Dermatology in General Medicine, 6th Edition, McGraw Hill, New York, 2003, pp. 137–149.

[2] I. Iwai, H. Han, L. den Hollander, S. Svensson, L.-G. Öfverstedt, J. Anwar, J. Brewer, M. Bloksgaard, A. Laloeuf, D. Nosek, S. Masich, L.A. Bagatolli, U. Skoglund, L. Norlén, The Human skin barrier is organized as stacked bilayers of fully extended ceramides with cholesterol molecules associated with the ceramide sphingoid moiety, J. Invest. Dermatol. 132 (9) (2012) 2215–2225, http://dx.doi.org/10.1038/jid.2012.43.

[3] M. Lundborg, A. Narangifard, C.L. Wennberg, E. Lindahl, B. Daneholt, L. Norlén, Human skin barrier molecular structure and function analyzed by Cryo-EM and molecular dynamics simulation, J. Struct. Biol. (2018) In press https://doi.org/10.1016/j.jsb.2018.04.005.

[4] L. Bartosova, J. Bajgar, Transdermal drug delivery in vitro using diffusion cells, Curr. Med. Chem. 19 (27) (2012) 4671–4677, http://dx.doi.org/10.2174/092986712803306358.

[5] R.C. Wester, X. Hui, T. Hartway, H.I. Maibach, K. Bell, M.J. Schell, D.J. Northington, P. Strong, B.D. Culver, In vivo percutaneous absorption of boric acid, borax, and disodium Octaborate Tetrahydrate in humans compared to in vitro absorption in human skin from infinite and finite doses, Toxicol. Sci. 45 (1) (1998) 42–51, http://dx.doi.org/10.1093/toxsci/45.1.42.

[6] E. Van Der Merwe, C. Ackermann, Physical changes in hydrated skin, Int. J. Cosmet. Sci. 9 (5) (1987) 237–247, http://dx.doi.org/10.1111/j.1467-2494.1987.tb00478.x.

[7] J.R. Bond, B.W. Barry, Limitations of hairless mouse skin as a model for in vitro permeation studies through human skin: hydration damage, J. Invest. Dermatol. 90 (4) (1988) 486–489, http://dx.doi.org/10.1111/1523-1747.ep12460958.

[8] A.C. Williams, B.W. Barry, Penetration enhancers, Adv. Drug Deliv. Rev. 64 (2012) 128–137, http://dx.doi.org/10.1016/j.addr.2012.09.032.

[9] R.J. Scheuplein, I.H. Blank, G.J. Brauner, D.J. Macfarlane, Percutaneous absorption of steroids, J. Invest. Dermatol. 52 (1) (1969) 63–70, http://dx.doi.org/10.1038/jid.1969.9.

[10] M. Sznitowska, S. Janicki, A. Baczek, Studies on the effect of pH on the lipoidal route of penetration across stratum corneum, J. Control. Release 76 (3) (2001) 327–335, http://dx.doi.org/10.1016/S0168-3659(01)00443-6.

[11] S.H. Moghadam, E. Saliaj, S.D. Wettig, C. Dong, M.V. Ivanova, J.T. Huzil, M. Foldvari, Effect of chemical permeation enhancers on stratum Corneum barrier lipid organizational structure and interferon alpha permeability, Mol. Pharm. 10 (6) (2013) 2248–2260, http://dx.doi.org/10.1021/mp300441c.

[12] Q.D. Pham, S. Björklund, J. Engblom, D. Topgaard, E. Sparr, Chemical penetration enhancers in stratum corneum — relation between molecular effects and barrier function, J. Control. Release 232 (2016) 175–187, http://dx.doi.org/10.1016/j.jconrel.2016.04.030.

[13] C. Hansch, P.P. Maloney, T. Fujita, R.M. Muir, Correlation of biological activity of phenoxyacetic acids with hammett substituent constants and partition coefficients, Nature 194 (4824) (1962) 178–180, http://dx.doi.org/10.1038/194178b0.

[14] M.T.D. Cronin, The Prediction of skin permeability using quantitative structure-activity relationship methods, in: J.E. Riviere (Ed.), Dermal Absorption Models in Toxicology and Pharmacology, CRC Press, 2005, pp. 113–134.

[15] I.T. Degim, W.J. Pugh, J. Hadgraft, Skin permeability data: anomalous results, Int. J. Pharm. 170 (1) (1998) 129–133, http://dx.doi.org/10.1016/S0378-5173(98)

00113-6.
[16] M.H. Fatemi, H. Malekzadeh, In silico prediction of dermal penetration rate of chemicals from their molecular structural descriptors, Environ. Toxicol. Pharmacol. 34 (2) (2012) 297–306, http://dx.doi.org/10.1016/j.etap.2012. 04.013.
[17] G. Lian, L. Chen, L. Han, An evaluation of mathematical models for predicting skin permeability, J. Pharm. Sci. 97 (1) (2008) 584–598, http://dx.doi.org/10.1002/jps.21074.
[18] R.O. Potts, R.H. Guy, Pharm. Res. 9 (5) (1992) 663–669, http://dx.doi.org/10.1023/A:1015810312465.
[19] S. Mitragotri, A theoretical analysis of permeation of small hydrophobic solutes across the stratum corneum based on scaled particle theory, J. Pharm. Sci. 91 (3) (2002) 744–752, http://dx.doi.org/10.1002/jps.10048.
[20] T.-F. Wang, G.B. Kasting, J.M. Nitsche, A multiphase microscopic diffusion model for stratum corneum permeability. I. formulation, solution, and illustrative results for representative compounds, J. Pharm. Sci. 95 (3) (2006) 620–648, http://dx.doi.org/10.1002/jps.20509.
[21] T. Wang, G.B. Kasting, J.M. Nitsche, A multiphase microscopic diffusion model for stratum corneum permeability. II. estimation of physicochemical parameters, and application to a large permeability database, J. Pharm. Sci. 96 (11) (2007) 3024–3051, http://dx.doi.org/10.1002/jps.20883.
[22] G.E. Crooks, Entropy production fluctuation theorem and the nonequilibrium work relation for free energy differences, Phys. Rev. E 60 (3) (1999) 2721–2726, http://dx.doi.org/10.1103/PhysRevE.60.2721.
[23] G.E. Crooks, Path-ensemble averages in systems driven far from equilibrium, Phys. Rev. E 61 (3) (2000) 2361–2366, http://dx.doi.org/10.1103/PhysRevE.61.2361.
[24] S. Park, K. Schulten, Calculating potentials of mean force from steered molecular dynamics simulations, J. Chem. Phys. 120 (13) (2004) 5946–5961, http://dx.doi.org/10.1063/1.1651473.
[25] I. Kosztin, B. Barz, L. Janosi, Calculating potentials of mean force and diffusion coefficients from nonequilibrium processes without Jarzynski's equality, J. Chem. Phys. 124 (6) (2006) 064106, , http://dx.doi.org/10.1063/1.2166379.
[26] L.Y. Chen, Nonequilibrium fluctuation-dissipation theorem of Brownian dynamics, J. Chem. Phys. 129 (14) (2008) 144113, http://dx.doi.org/10.1063/1. 2992153.
[27] C. Das, P.D. Olmsted, M.G. Noro, Water permeation through stratum corneum lipid bilayers from atomistic simulations, Soft Matter 5 (22) (2009) 4549–4555, http://dx.doi.org/10.1039/B911257J.
[28] R. Gupta, D.B. Sridhar, B. Rai, Molecular dynamics simulation study of permeation of molecules through skin lipid bilayer, J. Phys. Chem. B 120 (34) (2016) 8987–8996, http://dx.doi.org/10.1021/acs.jpcb.6b05451.
[29] Y. Masukawa, H. Narita, H. Sato, A. Naoe, N. Kondo, Y. Sugai, T. Oba, R. Homma, J. Ishikawa, Y. Takagi, T. Kitahara, Comprehensive quantification of ceramide species in human stratum corneum, J. Lipid Res. 50 (8) (2009) 1708–1719, http://dx.doi.org/10.1194/jlr.D800055-JLR200.
[30] M.H. Abraham, F. Martins, Human skin permeation and partition: general linear free-energy relationship analyses, J. Pharm. Sci. 93 (6) (2004) 1508–1523, http://dx.doi.org/10.1002/jps.20070.
[31] R.J. Scheuplein, Mechanism of percutaneous adsorption, J. Invest. Dermatol. 45 (5) (1965) 334–346, http://dx.doi.org/10.1038/jid.1965.140.
[32] R.J. Scheuplein, I.H. Blank, Mechanism of Percutaneous Absorption. IV. Penetration of Nonelectrolytes (alcohols) from Aqueous Solutions and from Pure Liquids, J. Invest. Dermatol. 60 (5) (1973) 286–296, http://dx.doi.org/10.1111/1523-1747.ep12723090.
[33] B. Idson, Vehicle effects in percutaneous absorption, Drug Metab. Rev. 14 (2) (1983) 207–222, http://dx.doi.org/10.3109/03602538308991389.
[34] M.W. Forney, L. Janosi, I. Kosztin, Calculating free-energy profiles in biomolecular systems from fast nonequilibrium processes, Phys. Rev. E 78 (5) (2008) 051913, , http://dx.doi.org/10.1103/PhysRevE.78.051913.
[35] B. Ongpipattanakul, R.R. Burnette, R.O. Potts, M.L. Francoeur, Evidence that oleic acid exists in a separate phase within stratum corneum lipids, Pharm. Res. 8 (3) (1991) 350–354, http://dx.doi.org/10.1023/A:1015845632280.
[36] F. He, W. Liu, S. Zheng, L. Zhou, B. Ye, Z. Qi, Ion transport through dimethyl sulfoxide (DMSO) induced transient water pores in cell membranes, Mol. Membr. Biol. 29 (3–4) (2012) 107–113, http://dx.doi.org/10.3109/09687688.2012.687460.
[37] D.A. van Hal, E. Jeremiasse, H.E. Junginger, F. Spies, J.A. Bouwstra, Structure of fully hydrated human stratum Corneum: a freeze-fracture Electron microscopy study, J. Invest. Dermatol. 106 (1) (1996) 89–95, http://dx.doi.org/10.1111/1523-1747.ep12328031.
[38] P.M. Elias, W.M. Holleran, K.R. Feingold, J. Tsai, G.K. Menon, The potential of metabolic interventions to enhance transdermal drug delivery, J. Invest. Dermatol. 7 (1) (2002) 79–85, http://dx.doi.org/10.1046/j.1523-1747.2002.19632.x.
[39] B.J. Aungst, N.J. Rogers, E. Shefter, Enhancement of naloxone penetration through human skin in vitro using fatty acids, fatty alcohols, surfactants, sulfoxides and amides, Int. J. Pharm. 33 (1) (1986) 225–234, http://dx.doi.org/10.1016/0378-5173(86)90057-8.
[40] C.K. Kim, J.-J. Kim, S.-C. Chi, C.-K. Shim, Effect of fatty acids and urea on the penetration of ketoprofen through rat skin, Int. J. Pharm. 99 (2) (1993) 109–118, http://dx.doi.org/10.1016/0378-5173(93)90352-G.
[41] K.B. Ita, Transdermal drug delivery: progress and challenges, J. Drug Deliv. Sci. Technol. 24 (3) (2014) 245–250, http://dx.doi.org/10.1016/S1773-2247(14)50041-X.
[42] S. Mitragotri, Y.G. Anissimov, A.L. Bunge, H.F. Frasch, R.H. Guy, J. Hadgraft, G.B. Kasting, M.E. Lane, M.S. Roberts, Mathematical models of skin permeability: an overview, Int. J. Pharm. 418 (1) (2011) 115–129, http://dx.doi.org/10.1016/j.ijpharm.2011.02.023.
[43] K. Vanommeslaeghe, E. Hatcher, C. Acharya, S. Kundu, S. Zhong, J. Shim, E. Darian, O. Guvench, P. Lopes, I. Vorobyov, A.D. Mackerell, CHARMM general force field: a force field for drug-like molecules compatible with the CHARMM all-atom additive biological force fields, J. Comput. Chem. 31 (4) (2010) 671–690, http://dx.doi.org/10.1002/jcc.21367.
[44] J.D. Yesselman, D.J. Price, J.L. Knight, C.L. Brooks 3rd, MATCH: an atom-typing toolset for molecular mechanics force fields, J. Comput. Chem. 33 (2) (2012) 189–202, http://dx.doi.org/10.1002/jcc.21963.
[45] G.S.K. Pilgram, J. van der Meulen, G.S. Gooris, H.K. Koerten, J.A. Bouwstra, The influence of two azones and sebaceous lipids on the lateral organization of lipids isolated from human stratum corneum, Biochim. Biophys. Acta Biomembr. 1511 (2) (2001) 244–254, http://dx.doi.org/10.1016/S0005-2736(01)00271-1.
[46] M. Clancy, J. Corish, O. Corrigan, A comparison of the effects of electrical current and penetration enhancers on the properties of human skin using spectroscopie (FTIR) and calorimetric (DSC) methods, Int. J. Pharm. 105 (1) (1994) 47–56, http://dx.doi.org/10.1016/0378-5173(94)90234-8.
[47] G. Embery, P.H. Dugard, The isolation of dimethyl sulfoxide soluble components from human epidermal preparations: a possible mechanism of action of dimethyl sulfoxide in effecting percutaneous migration phenomena, J. Invest. Dermatol. 57 (5) (1971) 308–311, http://dx.doi.org/10.1111/1523-1747.ep12292362.
[48] R. Notman, W.K. den Otter, M.G. Noro, W.J. Briels, J. Anwar, The permeability enhancing mechanism of DMSO in ceramide bilayers simulated by molecular dynamics, Biophys. J. 93 (6) (2007) 2056–2068, http://dx.doi.org/10.1529/biophysj.107.104703.
[49] S. Pronk, S. Páll, R. Schulz, P. Larsson, P. Bjelkmar, R. Apostolov, M.R. Shirts, J.C. Smith, P.M. Kasson, D. van der Spoel, B. Hess, E. Lindahl, GROMACS 4.5: a high-throughput and highly parallel open source molecular simulation toolkit, Bioinformatics 29 (7) (2013) 845–854, http://dx.doi.org/10.1093/bioinformatics/btt055.
[50] M.J. Abraham, T. Murtola, R. Schulz, S. Páll, J.C. Smith, B. Hess, E. Lindahl, GROMACS: high performance molecular simulations through multi-level parallelism from laptops to supercomputers, SoftwareX 1–2 (2015) 19–25, http://dx.doi.org/10.1016/j.softx.2015.06.001.
[51] U. Essmann, L. Perera, M.L. Berkowitz, T. Darden, H. Lee, L.G. Pedersen, A smooth particle mesh Ewald method, J. Chem. Phys. 103 (19) (1995) 8577–8593, http://dx.doi.org/10.1063/1.470117.
[52] B. Hess, H. Bekker, H.J.C. Berendsen, J.G.E.M. Fraaije, LINCS: a linear constraint solver for molecular simulations, J. Comput. Chem. 18 (12) (1997) 1463–1472, http://dx.doi.org/10.1002/(SICI)1096-987X(199709)18:12<1463::AID-JCC4>3.0.CO;2-H.
[53] S. Miyamoto, P.A. Kollman, Settle: an analytical version of the SHAKE and RATTLE algorithm for rigid water models, J. Comput. Chem. 13 (8) (1992) 952–962, http://dx.doi.org/10.1002/jcc.540130805.
[54] W.L. Jorgensen, J. Chandrasekhar, J.D. Madura, R.W. Impey, M.L. Klein, Comparison of simple potential functions for simulating liquid water, J. Chem. Phys. 79 (2) (1983) 926–935, http://dx.doi.org/10.1063/1.445869.
[55] J.B. Klauda, R.M. Venable, J.A. Freites, J.W. O'Connor, D.J. Tobias, C. Mondragon-Ramirez, I. Vorobyov, A.D. MacKerell, R.W. Pastor, Update of the CHARMM all-atom additive force field for lipids: validation on six lipid types, J. Phys. Chem. B 114 (23) (2010) 7830–7843, http://dx.doi.org/10.1021/jp101759q.
[56] R. Venable, A. Sodt, B. Rogaski, H. Rui, E. Hatcher, A. MacKerell Jr., R. Pastor, J. Klauda, CHARMM all-atom additive force field for sphingomyelin: elucidation of hydrogen bonding and of positive curvature, Biophys. J. 107 (1) (2014) 134–145, http://dx.doi.org/10.1016/j.bpj. 2014.05.034.
[57] B. Dahlén, I. Pascher, Molecular arrangements in sphingolipids. Thermotropic phase behaviour of tetracosanoylphytosphingosine, Chem. Phys. Lipids 24 (2) (1979) 119–133, http://dx.doi.org/10.1016/0009-3084(79) 90082-3.
[58] J. Stone, An Efficient Library for Parallel Ray Tracing and Animation, University of Missouri-Rolla, Master's thesis, Apr. 1998.
[59] W. Humphrey, A. Dalke, K. Schulten, VMD: visual molecular dynamics, J. Mol. Graph. 14 (1) (1996) 33–38, http://dx.doi.org/10.1016/0263-7855(96) 00018-5.
[60] M. Lundborg, E. Lindahl, Automatic GROMACS topology generation and comparisons of force fields for solvation free energy calculations, J. Phys. Chem. B 119 (3) (2014) 810–823, http://dx.doi.org/10.1021/jp505332p.
[61] N.M. O'Boyle, M. Banck, C.A. James, C. Morley, T. Vandermeersch, G.R. Hutchison, Open babel: an open chemical toolbox, Aust. J. Chem. 3 (1) (2011) 33, http://dx.doi.org/10.1186/1758-2946-3-33.
[62] S. Pronk, I. Pouya, M. Lundborg, G. Rotskoff, B. Wesén, P.M. Kasson, E. Lindahl, Molecular simulation workflows as parallel algorithms: the execution engine of Copernicus, a distributed high-performance computing platform, J. Chem. Theory Comput. 11 (6) (2015) 2600–2608, http://dx.doi.org/10.1021/acs.jctc.5b00234.
[63] I. Pouya, S. Pronk, M. Lundborg, E. Lindahl, Copernicus, a hybrid dataflow and peer-to-peer scientific computing platform for efficient large-scale ensemble sampling, Futur. Gener. Comput. Syst. 71 (2017) 18–31, http://dx.doi.org/10.1016/j.future.2016.11.004.
[64] M. Parrinello, A. Rahman, Polymorphic transitions in single crystals: a new molecular dynamics method, J. Appl. Phys. 52 (12) (1981) 7182, http://dx.doi.org/10.1063/1.328693.
[65] S.-J. Marrink, H.J.C. Berendsen, Simulation of water transport through a lipid membrane, J. Phys. Chem. 98 (15) (1994) 4155–4168, http://dx.doi.org/10.1021/j100066a040.
[66] M. Nategholeslam, C.G. Gray, B. Tomberli, Stiff spring approximation revisited: inertial effects in nonequilibrium trajectories, J. Phys. Chem. B 121 (2) (2017) 391–403, http://dx.doi.org/10.1021/acs.jpcb.6b08701.
[67] C.H. Bennett, Efficient estimation of free energy differences from Monte Carlo data, J. Comput. Phys. 22 (2) (1976) 245–268, http://dx.doi.org/10.1016/0021-9991(76)90078-4.